International Journal of Multiphysics
Volume 18, No. 1s, 2024
ISSN: 1750-9548

Test Analysis on Bearing Capacity of PHS Static Pressure Pile in Gravel Concrete Guiding-Hole

Jinsong Tu[1, 2], Gulei Chen[1], Rui Zhang[1, *]

1. College of Civil Engineering, Anhui Jianzhu University, Hefei, 230601, China

2. College of Architecture and Civil Engineering, West Anhui University, Lu'an, 237012, China

[*]Corresponding author jerry1604@163.com

Abstract

To address the construction challenges and insufficient bearing capacity issues associated with gravel soil static pressure prestressed high-strength concrete square (PHS) piles, this study introduces a refined gravel concrete guiding hole technique. This method is specifically applied to gravel soil static pressure PHS piles to enhance their bearing capabilities. The research involved designing a set of test piles for a particular engineering scenario in gravel soil. The construction process involved creating a pilot hole using a long spiral drill, followed by pouring C25 grade plain concrete and subsequently applying static pressure to form a 12m square pile. The load-bearing capacity of these piles was assessed through a combination of theoretical calculations, numerical simulations, and static load testing. The findings indicate that the implementation of concrete guiding-hole technology in PHS static pressure piles results in approximately a 60% increase in bearing capacity. This enhancement not only improves the foundational bearing capacity and stability but also contributes to the economic efficiency of the project. The enhanced bearing capacity, stability, and strength of the gravel soil static pressure PHS piles align with industry standards and specifications, underscoring the high feasibility of this approach.

Keywords: Gravel soil, spiral guiding-hole, PHS static pressure pile, ABAQUS numerical simulation, static load test

1. INTRODUCTION

In construction projects, inadequate bearing capacity of foundations can result in uneven settlement of buildings, potentially leading to structural damage [1]. To mitigate this issue, Liu et al. [2] emphasize in their research the importance of employing scientific foundation treatment methods. Such methods not only enhance the bearing capacity and economic efficiency of foundation treatments but also bolster the overall stability and service life of buildings. Prestressed high-strength concrete square (PHC) piles are increasingly utilized in foundation construction due to their notable benefits. These benefits include a high vertical bearing capacity, consistent quality, cost-effectiveness, and ease of production and transportation, as highlighted in various studies [3-5].

Numerous international studies have focused on the bearing capacity of prestressed high-strength concrete (PHC) piles. Liu et al. [6] introduced a variant of PHC piles reinforced with non-prestressing tendons, aimed at enhancing their performance in seismic areas. Comparative analyses of PHC piles with varying non-prestressing tendon ratios revealed that while the hysteresis characteristics and deformation capacity improved, the horizontal bearing capacity was compromised. In another study, Yao et al. [7] utilized Plaxis 2D software to develop a composite roadbed model for PHC piles. Their finite element analysis indicated that PHC piles capped at the top exhibited lower horizontal bearing capacity and poor disturbance resistance, leading to increased landslide risks. The longitudinal and transversal tie-beam structure was found to offer superior

stability. Additionally, Xu et al. [8] conducted a flexural test on single square piles with different reinforcement levels to enhance construction efficiency and reduce steel waste. Results showed that increasing the longitudinal reinforcement rate in single prestressed concrete solid square piles marginally improves their resistance to cracking and bending. Furthermore, Liang et al. [9] proposed a drain pile design featuring lateral openings on the pile body and an external geotextile wrapping, which accelerates consolidation time and enhances foundation bearing capacity.

Wang et al. [10] examined the impact of pile foundation type on structural design, emphasizing that the choice of pile foundation significantly influences design outcomes. Through site investigations, pile bearing capacity tests, and analysis of investigation reports, it was discovered that hollow square piles, when compared to tubular piles of similar side lengths and project costs, demonstrate higher bearing capacity and offer material savings for the foundation structure. Consequently, prestressed high strength (PHS) hollow square piles are identified as more economical, inheriting the advantageous characteristics of PHC piles. Additionally, Xu et al. [11] explored the influence of internal threads in pile walls on the pullout behavior of the pile core concrete. Utilizing acoustic emission technology for comprehensive damage monitoring, their tests revealed that the ultimate pullout capacity of pile core concrete with optimally spaced and depthed threads increased by 79%. This finding suggests that PHS hollow square piles are capable of enhancing the structural foundation's resistance to uplift loads.

Statkus et al. [12] conducted research on the settlement response of static pressure piles under vertical cyclic loads in sandy soils. Their study focused on determining the ratio of the maximum load to the ultimate bearing capacity, which exhibited minimal incremental settlement at the pile top. Concurrently, Liu and Sun et al. [13] acknowledged satisfactory outcomes with static compression piles in sandy soils but noted the necessity for further investigation into hole front parameters and end pressure. They also introduced the concept of guided hole static compression piles as a potential advancement. Moreover, Lu [14] identified several issues with traditional precast piles, such as the uplift of adjacent piles, challenges in penetrating medium-coarse sand layers, and difficulties in achieving the design depth, particularly under complex geological conditions. To address these problems, a combination of indoor modeling and numerical simulation was employed to examine the bearing characteristics of pilot hole implanted precast piles in such conditions. The findings indicate that pilot hole implanted precast piles effectively mitigate these challenges, offering a viable solution in complex geological settings.

Li et al. [15] formulated an effective construction plan for static pressure piles, integrating engineering examples with prevailing geological conditions. This approach yielded notable construction outcomes. The effectiveness of the guide hole static pressure pile process was evaluated in terms of inclination rate, settlement, and overall benefits, demonstrating its construction efficacy.

Kou et al. [16] executed a comprehensive field investigation to assess the residual forces in PHC pipe piles in Hangzhou, China. The findings indicated an exponential increase in residual force along the pile length up to the neutral plane, followed by a decrease towards the pile tip. This significant residual force profoundly influences the evaluation of pile load distribution, consequently affecting axial and toe resistance. Concurrently, Zhu et al. [17-18] observed in their static load tests of immersed piles that pile end resistance escalates non-linearly with both increasing settlement and pile length. Furthermore, they noted that the proportion of pile end resistance to the total load at the pile top diminishes as the pile length increases. In a separate study, Budek et al. [19] conducted a parametric analysis on hollow precast prestressed pipe piles to examine the effects of soil external confinement on the pile shaft. The outcomes revealed a consistent pattern of structural damage, predominantly compressive, occurring at similar displacement levels across all model piles, regardless of parameter variations. Additionally, Kai [20] utilized ANSYS for finite element simulations to analyze the static load compressive behavior of prestressed concrete pipe piles. This was complemented by a single-pile static load compressive performance test on a prestressed concrete pipe pile, providing a comprehensive understanding of the pile's structural response under compression.

The ultimate bearing capacity of piles is significantly influenced by variables such as pile type, soil type, and construction technique, making the precise computation of this capacity a critical issue in geotechnical engineering [21-23]. This paper presents a detailed analysis, incorporating static load tests and finite element analysis, to determine the bearing capacity of PHC pipe piles and guide hole static compression piles. It specifically examines the bearing capacities of prefabricated piles in gravel soil and pebble-bearing layers within an urban context. In this study, long spiral guide hole precast static pressure piles were employed as a foundational treatment method. Notably, the experimental approach adopted here involved a more extended loading duration, smaller incremental loads, and more stages of loading compared to previous tests. This methodology resulted in more precise settlement measurements, thereby offering more valuable insights for guiding practical engineering applications.

2. MATERIAL AND RESEARCH METHOD

2.1 Test site conditions

This research focuses on the bearing capacity of guiding-hole PHS static pressure piles in gravel geology. It integrates the geological conditions specific to a city university's science and technology building project. The study adopts the static load test methodology as outlined by Kai. Data regarding the stratigraphy were derived from the project's geotechnical engineering investigation report and aligned with the standards specified in the "Technical Code for Building Pile Foundations [24]." This comprehensive analysis facilitated the acquisition of detailed soil layer characteristics, which are systematically presented in Table 1.

Table 1: Mechanical parameters of the soil layer

Name of soil layer	Type of soil	Thickness(m)	Ultimate shaft resistance (kPa)	Ultimate tip resistance (kPa)	Cohesion(kPa)	Angle of internal friction (°)	Modulus of deformation (MPa)
Miscellaneous fill	Soft and weak soils	1.2	20	-	5	8	3.0-3.5
Fine Sand	Weak-medium soft soil	4.1	26	-	6	15	7.0
Pebbles with medium coarse sand (medium dense state)	Medium-hard soils	4.65	90	6000	5	20	10.0
Pebbles with medium coarse sand (dense state)	Medium-hard soils	-	110	8000	3	17	15.0

2.2 Test Pile Construction Process

In the foundation treatment of this project, the gravel soil concrete guiding-hole PHS static pressure pile was utilized. A long auger drilling machine drilled a hole with a diameter of 650mm. Drilling was paused upon reaching the designed pile depth. Concurrently, as the auger machine was retracted and the soil discharged, a concrete pump was employed to infuse C25 fine gravel commercial concrete into the hole. This process continued until the drilling tool was completely withdrawn from the hole. This methodology is illustrated in Fig.1.

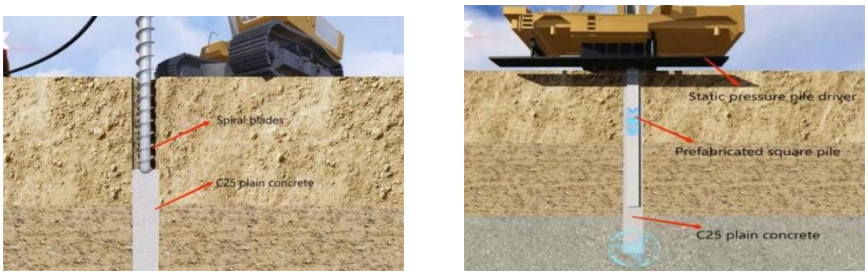

(a) (b)

Figure 1: (a) Guiding-hole construction (b) Static pressure pile construction

Upon completion of the long spiral guiding hole, the static pile driving operation is initiated before the initial setting of the newly poured C25 concrete, typically within approximately 1.5 hours. The static pile driver positions and then drives the C80 strength PHS square piles, each with a side length of 450mm, into the soil, ensuring they reach the designed top elevation.

The construction technique of long spiral guiding-hole static pressure precast piles is recognized for its cost-effectiveness and reliability, along with its low noise and vibration levels. However, there exists some uncertainty regarding its load-bearing capacity. To address this, the current study undertakes an assessment of the long spiral guiding-hole static pressure precast pile. This includes theoretical calculations of bearing capacity, destructive static load testing, and ABAQUS simulations for bearing capacity evaluation.

2.3 Test loading program

2.3.1 Test equipment

The necessary instruments for the test are detailed in Table 2.

Table 2: Test equipment

equipment name	Models	Management Number	Factory number	Verification Certificate No	Valid for inspection until
Static load tester	JCQ-503B	S11423	1711586	HF22AA041710048G	2023/7/25
Displacement sensor	upm-50	S11564	711699	HF22AA041710049	2023/7/25
Displacement sensor	upm-50	S11565	712024	HF22AA041710050	2023/7/25
Hydraulic jack	800T	S11675	20042602	AVV20225431748	2023/06/21

2.3.2 Loading Program

The vertical compressive static load test on this single pile was executed using the counterforce method with a compression weight platform, employing a slow sustaining load approach. The foundation pile for this project, as depicted in Fig. 2, has a designated cross-sectional dimension, and its length extends to 12 meters. Notably, during the test, the maximum load applied was not capped and continued to increase until the test pile sustained damage.

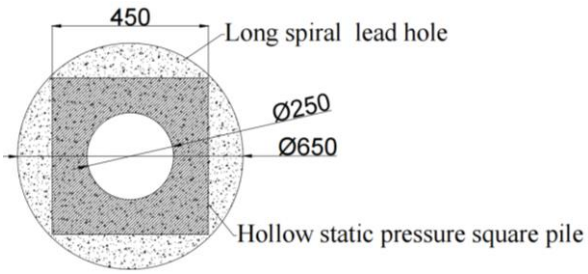

Figure 2: Cross-sectional drawing of long spiral guiding-hole static pressure pile

The loading procedure for the test was segmented into 15 distinct stages, with each stage involving equal incremental loading. The graded load applied at each stage was set at one-tenth of the design value for the vertical compressive capacity of the PHS prefabricated square pile. Each loading stage was maintained for a duration of 120 minutes. Notably, the initial loading stage involved a load double the amount of the standard graded load. Settlement measurements were recorded at the conclusion of each loading stage. The application of the subsequent load level was contingent upon the settlement rate at the pile top meeting the established criterion for relative stability.

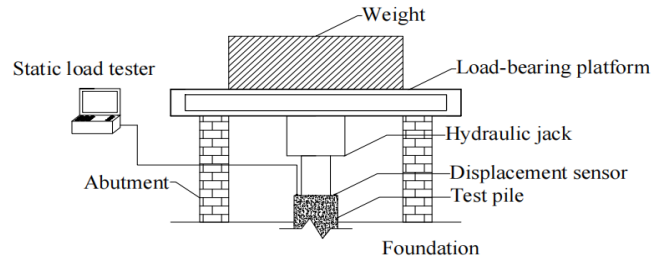

Figure 3: Loading diagram for static load test

2.3.3 Uninstallation program

In the testing protocol, the unloading for each stage was set at twice the amount of the corresponding loading phase. During unloading, each load level was sustained for a duration of one hour. The procedure for progressing to the next load level involved measuring and recording the pile top's settlement at specific intervals: the 15th minute, 30th minute, and 60th minute. Upon reaching zero load during unloading, the residual settlement of the pile top was measured and recorded. This residual settlement monitoring phase was maintained for no less than three hours, with measurements taken at the 15th minute, 30th minute, and subsequently at every 30-minute interval to accurately capture the residual settlement of the pile top.

2.4 Design and theoretical load capacity calculation of guiding-holes concrete static press piles

The design and theoretical calculations of guiding-hole concrete static press piles primarily employ two methodologies:

(1) Utilizing the guidelines from the "Technical Code for Building Pile Foundations [24]", the design value of a monopile's vertical bearing capacity is ascertained through an empirical relationship that correlates the soil's physical indices with bearing capacity parameters. This design value is instrumental in determining the graded load values requisite for static load testing and finite element numerical simulations. The mechanical properties of the soil layers are detailed in Table 1, while Table 3 provides the geometric and mechanical parameters of the C80 precast concrete square piles.

Table 3: Geometric parameters of precast pile

Name	Size(mm*mm)	Pile length(m)	Concrete strength Grade	Density (t/m^3)	Young's modulus(kPa)	Poisson's ratio
Precast concrete square pile	450*450	12	C80	2.5	$3.8*10^7$	0.25

According to equation (1) in the Technical Code for Building Pile Foundations [24]:

$$Q_{uk} = Q_{sk} + Q_{pk} = u\sum q_{sik} L_i + q_{pk} A_p \quad (1)$$

where: Q_{uk} - ultimate vertical bearing capacity of a single pile; Q_{sk} , Q_{pk} k-standard values of total ultimate shaft resistance and total ultimate tip resistance of single pile; u -pile circumference; q_{sik} -standard value of ultimate shaft resistance for soil layer i of a single pile; L_i -the length of the pile in the ith soil layer; q_{pk} -Standard value of ultimate tip resistance of a single pile; A_p -Pile end area.

(2) The Schmertmann method [25] is employed to deduce the bearing capacity distribution of the soil. This method involves the calculation of key parameters including Relative Bearing Capacity (RBC), Relative Bearing Area (RBA), and Equivalent Earth Pressure (EEP). These parameters are determined using specific equations designated as Eqs. (2)-(4), which are integral to the Schmertmann method for accurately assessing the soil's bearing capacity profile.

$$\mathrm{RBC} = (0.1 + 0.015 \times \mathrm{N}_{60}) \times \mathrm{N}_{\gamma} \tag{2}$$

$$\mathrm{RBA} = (0.8 + 0.20 \times (\mathrm{D}_f / \mathrm{D}_p)) \times (\mathrm{B}_f / \mathrm{B}_p) \tag{3}$$

$$\sigma_{eq} = \gamma^{*} \times (H_f + H^{'}) \tag{4}$$

where, N_{60} is the standard penetration value determined by the Standard Penetration Test, N_{γ} is the Volumetric weight adjustment factor for the soil, D_f is the diameter of the load-applied rebar hammer, D_p is the diameter of the hole in the rebar hammer, B_f is the length of the reinforcing hammer to which the load is applied, B_p is the hole range of the rebar hammer, γ^{*} is the adjusted soil weight, H_f is the depth of penetration of the rebar hammer, $H^{'}$ is the effective pore water pressure in the upper soil layer.

Employing the equations specified earlier, it becomes feasible to calculate the values of Relative Bearing Capacity (RBC), Relative Bearing Area (RBA), and Equivalent Earth Pressure (EEP). These calculated values are then utilized to determine the bearing capacity distribution of the soil, providing a comprehensive understanding of its load-bearing characteristics.

Consequently, by applying these methodologies and calculations, the standard value for the ultimate bearing capacity of a single C80 precast concrete square pile is determined to be 3208.68 kN.

2.5 Pile theoretical bearing capacity analysis of gravel soil guiding-hole

Utilizing the long spiral guiding hole technique to fill with C25 fine stone commercial concrete, and considering the guiding-hole diameter of 650mm in accordance with equation (1) from the "Technical Code for Building Pile Foundations [24]," the standard value of the ultimate bearing capacity for a single guiding-hole pile is calculated to be 4454.69 kN.

2.6 Theoretical bearing capacity analysis of composite stiff piles in sand and gravel soil

Upon the infusion of C25 fine stone concrete into the long spiral guiding hole and subsequent pressing of the C80 precast square pile using a static pile driver, a composite pile is created. The theoretical bearing capacity of this composite pile is calculated in accordance with equations (5)-(7) as specified in the "Technical Code for Building Pile Foundations [24]

$$\mathrm{Q}_{uk} = u \sum \alpha_{sik} q_{sik} L_i + \beta_p \theta q_{pk} A_p \tag{5}$$

$$\alpha_{sik} = (0.8 / d)^{1/3} \tag{6}$$

$$\beta_p = (0.8 / D)^{1/3} \tag{7}$$

where: The meaning of the symbol is the same as that of formula 1. α_{sik}, β_p - adjustment factor for shaft resistance and adjustment factor for tip resistance of soil layer i in the outer core of the composite section of a strong composite pile; θ - reduction factor for bearing capacity of natural foundation soil at the end of strong composite piles. D, d -pile outer diameter, pile inner diameter.

Consequently, following the specified calculations in the "Technical Code for Building Pile Foundations [24]", the bearing capacity of the composite pile is determined to be 6718.77 kN.

2.7 Analysis of theoretical pile bearing capacity of precast pile formation in gravel soil

Based on theoretical calculations, the bearing capacity of a precast square pile in sand and gravel soil is approximately 3208.68 kN, while that of a gravel soil guiding-hole pile is around 4454.69 kN. The bearing capacity of a composite static pile in sand and gravel soil is estimated to be about 6718.77 kN. However, referring to the experimental findings of Wei et al. [26], the design value for the vertical bearing capacity of a single pile can be pragmatically set at 3800 kN.

3. RESULTS AND ANALYSIS

To further investigate the ultimate load capacity of gravel soil static piles, this paper details a static load test conducted on test piles. Static load testing is the most reliable method for determining the vertical compressive bearing capacity of an individual pile in a pile foundation, as it accurately accounts for geological and pile body factors. This test allows for the determination of the relationship between the loading value (Q) and the vertical displacement at the pile top (Settlement). To better visualize this relationship, a Q-s curve is developed.

The static load test was performed on three 12-meter engineering foundation piles, referred to as test piles A, B, and C. The applied graded load was set at 1/10 of the pile's design vertical bearing capacity, equivalent to 380 kN. The initial stage of loading was double the graded load, amounting to 760 kN. Similarly, the unloaded graded load was set at twice the loaded graded load, which is also 760 kN. The loading scheme followed the procedures outlined in section 2.3.

3.1 Test data

The execution of the destructive static load test on the three test piles (A, B, and C) resulted in the collection of comprehensive data, including load values, displacement at each loading level, and cumulative displacement for each of the test piles. This data is systematically compiled and presented in Figures 4, 5, and 6, offering a detailed visual representation of the test outcomes.

3.2 Analysis of results

The presented data reveals that test piles A and C underwent a segmented loading process comprising 15 levels, alongside eight distinct levels of unloading, each culminating in a maximum test load bearing capacity of 6080kN. In contrast, test pile B was subjected to a similar 15-level loading procedure, also achieving a maximum test load bearing capacity of 6080kN.

International Journal of Multiphysics
Volume 18, No. 1s, 2024
ISSN: 1750-9548

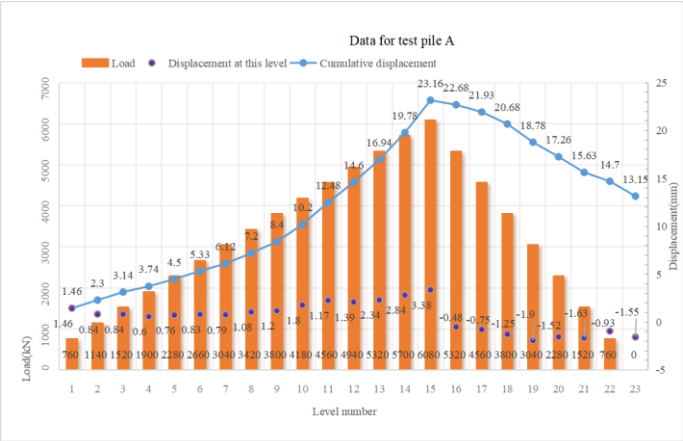

Figure 4: Data for test pile A

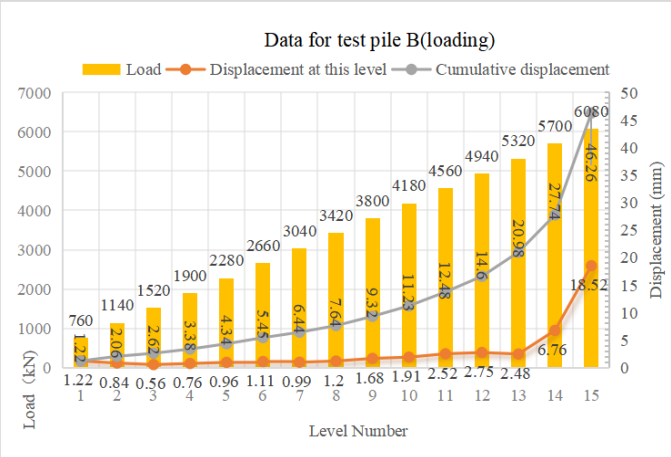

Figure 5: Data for test pile B

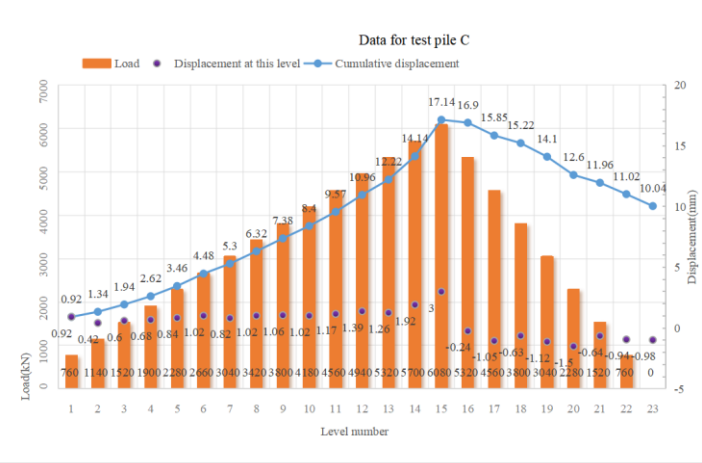

Figure 6: Data for test pile C

Pearson correlation coefficients in Equation (8) between two variables (Loads and Cumulative displacement) are calculated [27],

$$r = \frac{\sum_{i=1}^{n}(X_i - \overline{X})(Y_i - \overline{Y})}{\sqrt{\sum_{i=1}^{n}(X_i - \overline{X})^2}\sqrt{\sum_{i=1}^{n}(Y_i - \overline{Y})^2}} \tag{8}$$

where X_i; and Y_i; are variables, $\overline{X}$ and $\overline{Y}$ are their mean values, and n is the total number of data points.

As shown in Table 4, Pearson correlation coefficients in equation (8) between two variables (Loads and Cumulative displacement).

Table 4. Pearson correlation coefficients

Piles Name	Pearson correlation coefficients
Pile A	0.9667
Pile B	0.9528
Pile C	0.9900

According to the results of the calculations, there is a strong correlation between the two variables (Loads and Cumulative displacement).

3.2.1 Displacement analysis at this level

During the loading phase of test pile A, the displacement at this level exhibited a consistent decrease as the load increased from 760kN to 1900kN. Subsequently, the displacement tended to increase continuously with further load increments from 1900kN to 6080kN. The minimum displacement at this level was recorded when the load reached 1900kN, while the maximum displacement was observed at the highest load of 6080kN. The maximum differential in displacement at this level was determined to be 2.78mm.

In the loading phase of test pile C, there was a continuous decrease in displacement at this level as the load increased from 760kN to 1140kN. Following this, the displacement exhibited an approximate continuous increase from 1140kN to the peak load of 6080kN. The minimum displacement at this level was observed at 1140kN, measuring 0.42mm, while the maximum displacement occurred at 6080kN. The maximal differential in displacement recorded at this level was 2.58mm.

In the loading phase of test pile B, the displacement at this level showed a consistent decrease with the load increasing from 760kN to 1520kN. After reaching 1520kN, the displacement tended to increase approximately continuously up to the maximum load of 6080kN. The smallest displacement at this level was recorded at a load of 1520kN, measuring 0.56mm, whereas the largest displacement was observed at the peak load of 6080kN. The maximum displacement difference noted at this level was 17.96mm.

The initial displacement trends of the three test pile groups display a similar pattern of decrease under small loads. This behavior is hypothesized to originate from inherent defects within the piles, such as minor voids and holes. These imperfections undergo compaction in this early phase, which in turn marginally enhances the overall compressive resistance of the piles [28-29].

During the unloading phase of test pile A, the displacement at this level increased continuously as the unloading value decreased from 5320kN to 3040kN, and subsequently tended to decrease when the unloading value reduced from 3040kN to 0kN. The smallest displacement at this level, 0.48mm, was observed when unloading to 5320kN, while the largest displacement, 1.9mm, occurred at an unloading value of 3040kN. The maximum displacement difference at this level was 1.42mm.

In the unloading phase of test pile C, the displacement at this level varied, showing three instances of continuous increase and two of decrease. The smallest displacement, measured at 0.24mm, was recorded when unloading to

5320kN, and the largest displacement, 1.5mm, was observed when unloading to 2280kN. The maximum displacement difference at this level was 1.26mm.

3.2.2 Q-s curve analysis

The Q-s curve depicted in Fig 7 for test pile A during the loading process is characterized by a parabolic shape. As the load increases, the settlement continues to rise without any significant deviations in the middle section of the curve. In contrast, during the unloading process, the Q-s curve assumes a zigzag pattern, maintaining an approximately linear relationship. Notably, the curve does not revert to its original position after unloading.

The maximum deformation value observed during loading was 23.16mm, which occurred at the 16th loading level with a load of 6080kN. After complete unloading, a residual deformation of 13.15mm was recorded at the 23rd level.

This behavior aligns with the principles outlined in equation (9) of the Technical Code for Building Pile Foundations [24].

$$S_r = S_2 / S_1 \tag{9}$$

where: S_r -Resilience and deformation rate of pile foundation; S_1 -The maximum deformation value during loading; S_2 -Residual deformation after complete unloading.

The resilience and deformation rate of the pile foundation are calculated to be 56.78%. This indicates a general trend of stability in the deformation characteristics, with no significant or abrupt increases or decreases observed. In accordance with the relevant specifications, the ultimate vertical compressive bearing capacity of the test pile is determined to be no less than the maximum test load of 6080kN. This finding confirms that the precast pile adheres to the industry standards as stipulated in the specifications for vertical compressive static load testing of a single pile.

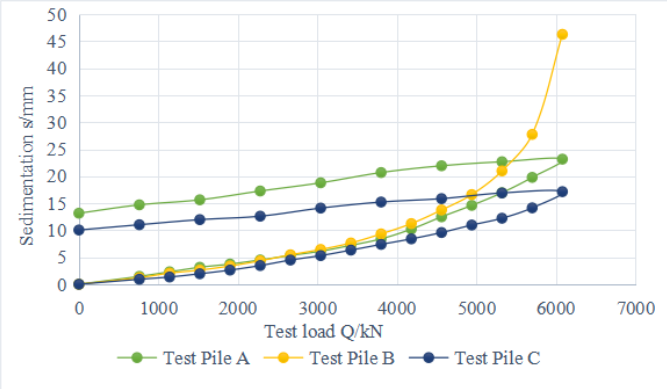

Figure 7: Q-s curve

During the loading phase of test pile B, the Q-s curve exhibits a parabolic shape. As the load increases, the settlement correspondingly rises. Notably, when the load increment ranges from 5700kN to 6080kN, the settlement demonstrates a marked, albeit ineffective, increase. The peak displacement recorded is 46.26mm, occurring at the 16th loading level with a load of 6080kN. This displacement at the 16th level is over double that at the 15th level, failing to meet the relative stability criterion, which necessitates the termination of loading. Consequently, the vertical compressive capacity of a single pile for test pile B is determined to be at the previous load level, specifically at the maximum test load of 5700kN.

During the loading phase of test pile C, the Q-s curve maintained an approximately linear trajectory, with the settlement consistently increasing in tandem with the load. There were no significant fluctuations in the middle section of the curve. In the unloading phase, the Q-s line exhibited a zigzag pattern while still maintaining an approximate linearity. Notably, the curve did not revert to its original position post-unloading. The maximum

displacement observed was 17.14mm, occurring at the 16th loading level with a load of 6080kN. The most pronounced rebound was recorded upon unloading to the 23rd level, where the settlement reverted to 10.04mm, yielding a rebound rate of 41.42%. The overall trend displayed minor fluctuations with no abrupt increases or decreases. In accordance with the specified standards, the ultimate vertical compressive bearing capacity of the test pile is ascertained to be no less than the maximum test load of 6080kN. This confirms that the precast pile meets industry specifications and adheres to the standard practices for vertical compressive static load testing of a single pile.

3.2.3 Accuracy analysis

In the static load tests conducted on the three test piles, the overall settlement trend closely parallels that observed in Kai's static load test [20]. This test featured a longer loading duration, smaller incremental loads, more stages of loading, leading to more precise measurements of settlements. Despite having identical dimensions and materials, the piles exhibited varying settlements under the same loading conditions. Pile B showed the largest settlement, pile C the smallest, and pile A's settlement was comparatively average. Factors such as testing equipment, environmental conditions, and human involvement might contribute to these discrepancies. Owing to its more representative and average settlement, pile A is chosen for comparison with the model piles in the finite element numerical analysis, to verify the accuracy of the static load test.

3.3 Finite element numerical analysis of bearing capacity of static press precast piles in sand and gravel soil

For an in-depth examination of the bearing capacity of concrete guiding-hole PHS (Prestressed High Strength) static pressure piles in gravel soil, a soil and pile body model was developed using ABAQUS, in accordance with the process and geological data. This modeling facilitated the creation of a monopile representation within the soil layer. Upon applying the load to this model, a finite element numerical simulation was conducted. The results from this simulation were then juxtaposed with theoretical calculation values and outcomes from static loading tests. The primary objective of this comparison was to assess the bearing capacity of the pilot hole static pile and determine whether it aligns with the specifications, as established through finite element analysis.

3.4 Computing Fundamentals

The numerical simulation of the pile foundation's bearing capacity is segmented into three distinct simulations: the numerical simulation of the precast hollow square pile within soil (termed the pile-soil model), the simulation evaluating the bearing capacity with the frictional interaction between the precast hollow square pile and C25 concrete (designated as the pile-C25 concrete model), and the simulation considering the precast square pile and C25 concrete as a unified entity (referred to as the overall situation) [30].

In these simulations, parameters for each element are based on actual conditions and data derived from the survey report. A notable aspect is that the elastic modulus of the pile body is substantially greater than that of the soil. Therefore, the following assumptions, outlined in Wu's paper [28], are employed:

Piles are regarded as elastic materials, characterized by continuity, homogeneity, isotropy, and are unaffected by shrinkage, creep, or elastic-plastic cracking of the concrete.

Soils are considered as continuous, homogeneous, isotropic materials, with soil particles being incompressible.

A face-to-face contact approach is used for the interaction surfaces between the pile and the soil.

The behavior of the soil surrounding the piles is modeled using the Mohr-Coulomb model.

Temperature variations are not taken into account in the simulation process.

3.5 Computational Models

3.5.1 Modeling and Attribute Definition

The numerical simulation for assessing the bearing capacity primarily involves the creation of two models: one for the soil body and another for the pile body [28, 31]. The dimensions of the soil body model are 9m x 9m x 24m, and it is segmented into three distinct layers. The geometric and material properties of each soil layer are

detailed in Table 1. Similarly, the geometric dimensions and material properties of the prefabricated square piles are outlined in Table 3. The guiding-hole, employed in the construction process, is characterized by a diameter of 650mm and a length of 12m.

For the soil model, conventional constraints are applied to its four sides, with total constraints on its bottom surface. The interaction between the soil and pile bodies is configured as a face-to-face contact. In this setup, the side surface of the pile body is designated as the primary contact surface, while the corresponding surface on the soil body serves as the slave contact surface. The contact properties at the pile-soil interface are defined in terms of tangential and expected behaviors. The tangential behavior is governed by penalty friction, with the friction coefficient set at 0.3. The expected behavior is defined as "hard" contact, ensuring a realistic simulation of the interaction dynamics between the pile and the soil.

3.6 Grid division

The soil in the simulation is segmented into 3267 elements, while the pile model for the precast hollow square pile is divided into 3724 elements. The pile model representing the interaction of the pile with C25 concrete comprises 3163 elements, and the model simulating the overall situation, where the precast square pile and C25 concrete are considered as a single unit, consists of 5280 elements. The specific details of the meshing for each model are illustrated in Figure 8, providing a clear visual representation of the division and arrangement of elements within each model.

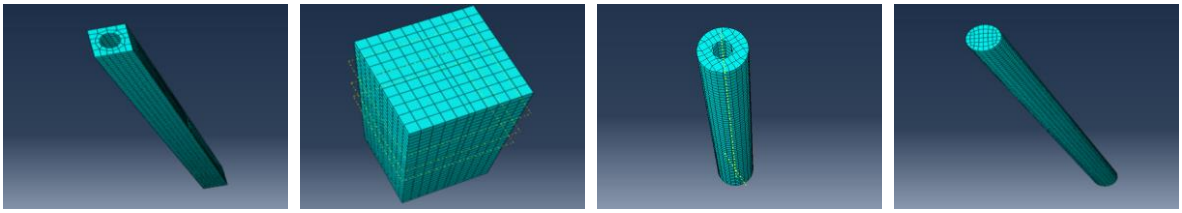

(a) (b) (c) (d)

Figure 8: (a) Grid division of precast square pile (b) Soil mesh division diagram (c) Pile concrete model meshing diagram (d) Overall situation grid division diagram

3.7 Data collation

For the pile-soil model, the loading sequence is configured into 17 analysis steps. This includes two initial steps for analyzing ground stress and 15 subsequent steps for load analysis. The loading process is structured into 15 levels, with each level incrementing the load by an amount equivalent to 1/10th of the design value for the vertical compressive bearing capacity of a single pile, which equates to 380kN.

The initial loading phase commences with a load that is twice the design value of the vertical compressive bearing capacity of a single pile, amounting to 760kN. This loading is progressively increased in the defined increments, continuing until the pile body experiences damage. This systematic approach allows for a detailed and nuanced understanding of the pile's response to increasing loads, ultimately providing insights into its structural integrity and capacity.

3.8 Data collation and analysis

The numerical simulation of the bearing capacity was conducted for three distinct models: the pile-soil model, the pile-concrete model, and the overall situation model. Each simulation was carried out using ABAQUS to determine the settlement behavior of the precast pile under varying load conditions.

For the pile-soil model, when a load of 3800kN was applied, the pile model exhibited no significant deformation. At a higher load of 4560kN, the settlement of the pile model increased significantly, and upon reaching the destructive load of 6080kN, the settlement peaked at 46.872mm.

In the simulation of the pile-concrete model, similar behavior was observed. With a 3800kN load, the pile model showed no noticeable deformation. However, at 5320kN, the settlement increased significantly, and at the destructive load of 6080kN, the maximum settlement was 26.258mm.

For the overall situation model, the pile model displayed no apparent deformation at a load of 3800kN. As the load was increased to 5320kN, the settlement of the pile model again increased significantly, and at the destructive load of 6080kN, the settlement reached its maximum at 20.442mm.

The displacement change curve revealed that the first half of the curve maintained a linear form, with no apparent rise or fall in the middle. The second half of the curve assumed an approximately parabolic shape, devoid of any folding lines. The vertical compressive ultimate bearing capacity of the single pile in each model was not less than the maximum applied load of 6080kN, satisfying the requirements for bearing capacity.

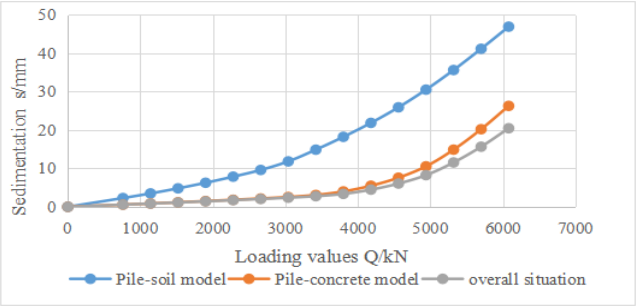

Figure 9: Curve of variation of pile settlement with comparison

3.9 Accuracy analysis

Kai [20] compares the vertical load-settlement curve obtained from tests with the results of finite element calculations. The comparison reveals that while the development trends of the two are similar, there is a discernible margin of error. This discrepancy is attributed to factors such as the pile head and base [32].

Similarly, in the analysis of the bearing capacity of the long spiral guiding-hole static pressure pile, discrepancies are observed between theoretical calculations, numerical simulations, and static load tests. These errors may stem from various sources, including the mesh division in the simulation, the interaction between the precast pile and C25 concrete during extrusion, among other factors. These inherent uncertainties highlight the complexities involved in accurately simulating and predicting pile behavior under load conditions.

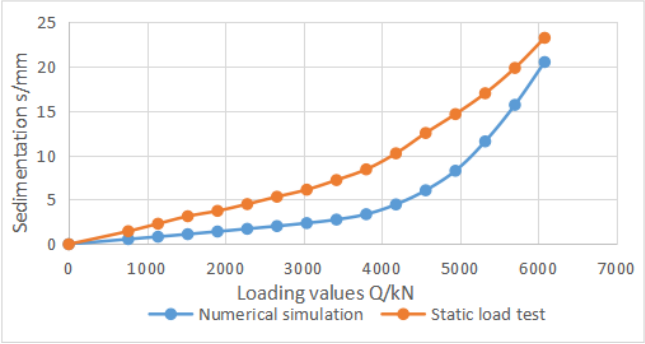

Figure 10: Comparison curves of numerical simulation and static load test

Using Formula (6), a step-by-step error analysis is conducted:

$$D_i = [2 \times (| N_i - S_i | / (N_i + S_i)] \times 100\% \quad (9)$$

where: D_i -The relative difference between the test pile A and The numerical simulation of the model pile. i -The order of level number. N_i -settlement of the numerical simulation of the model pile under order i load. S_i -settlement of the test pile A under order i load.

The relative difference achieves its maximum value of 69.39% when the load is at the 11th increment, while the minimum value of 12.45% is observed at the 15th increment. Despite the noted discrepancies between the mathematical model's pile load test evaluation method and the failure load [33], it is deducible that the error margin falls within an acceptable range. Consequently, this finite element numerical analysis pertaining to the bearing capacity of gravel soil static precast piles substantiates the validity of the static load test results.

4. CONCLUSIONS

Theoretical Analysis: Theoretical calculations indicate that the bearing capacities for various pile types in gravel soil are as follows: prefabricated square pile at approximately 3208.68 kN, bored pile at about 4454.69 kN, and composite static pressure pile at roughly 6718.77 kN. Notably, the composite static pressure pile exhibits a significantly higher theoretical bearing capacity compared to the prefabricated square pile and bored pile, aligning well with industry usage standards.

Static Load Testing: In the vertical compressive static load test conducted on three test piles, upon incrementally increasing the load to 6080 kN, test piles A and C showed no damage, whereas test pile B exhibited increasing settlement. The Q-S curves for piles A and C displayed no significant fluctuations, suggesting their ultimate vertical compressive bearing capacities are at least 6080 kN. For test pile B, its capacity is inferred to be no less than 5700 kN, the load preceding the maximum test load.

Numerical Simulation: In the ABAQUS-based load capacity simulation for gravel soil concrete pilot hole PHS static piles, the piles displayed negligible deformation. The displacement change curve generally followed a parabolic trajectory, with no abrupt increases or decreases throughout. Upon application of the maximal load of 6080 kN, the pile settlement peaked, indicating that the ultimate vertical compressive load capacity of these piles is at least 6080 kN.

Comparative Analysis: When comparing the foundation treatment methods of static pressure PHS piles and guiding-hole grouted piles, it is evident that the long spiral guiding-hole static pressure pile is versatile, suitable for gravel soil, and effectively mitigates the extrusion effect associated with static piles. This method also omits the need for excavation and soil burying, leading to reduced construction time and costs. Moreover, it offers enhanced bearing capacity, stability, and strength, yielding significant economic benefits while adhering to industry standards and specifications, thereby confirming its high feasibility.

DATA AVAILABILITY

The data used to support the findings of this study are included within the article.

DISCLOSURE

However, the opinions expressed in this paper are solely of the authors.

DECLARATION OF COMPETING INTEREST

The authors declare that they have no known competing financial interests or personal relationships that could have appeared to influence the work reported in this paper.

ACKNOWLEDGMENTS

This work was supported in part by the Key Research and Development Technology Project of Anhui Province under Grant 2022l07020005, and in part by the Major Project of Natural Science Research in Anhui Universities under Grant KJ2020A0627. Horizontal Projects-Talent Startup Fund Project of West Anhui University WGKQ2022021.Integrated Application of Comprehensive Information Modeling for Whole Life Cycle Buildings Based on BIM and 5G Technologies 0045023055.Science and Technology Program of Anhui

Department of Housing and Construction. Research and Suggestions on Vigorously Developing Green Assembly Building Industry in Anhui Province.

REFERENCE

[1] Sun, X.L., “Non-uniform settlement reinforcement technique for static pile construction of building pile foundation (in Chinese)”, New Technology and New Products of China, 2022 (17): p. 125-127. DOI: https://doi.org/10.13612/j.cnki.cntp.2022.17.017

[2] Liu, S.Y., Zhou, J., Zhang, D.W., Ding, X.M., Lei, H.Y., “State of the art of the ground improvement technology in China”, China Civil Engineering Journal, 2020, 53(4): p.93-110. DOI: https://doi.org/10.15951/j.tmgcxb.2020.04.009

[3] Joen, P., Park, R., “Analysis of spirally reinforced prestressed concrete piles”, PCI Journal, 1990, 35(4): p. 54-83. DOI: https://doi.org/10.15554/pcij.07011990.54.83

[4] Yang, Z. X., Guo, W. B., Zha, F. S., Jardine, R. J., Xu, C. J., & Cai, Y. Q., “Field behavior of driven prestressed high-strength concrete piles in sandy soils”, Journal of Geotechnical and Geoenvironmental Engineering, 2015, 141(6): p. 04015020. DOI: https://doi.org/10.1061/(ASCE)GT.1943-5606.0001303

[5] Tan Y, Lin G., “Comprehensive load test on prestressed concrete piles in alluvial clays and marl in savannah, Georgia”, Journal of Performance of Constructed Facilities, 2014, 28(1): p. 178-190. DOI: https://doi.org/10.1061/(asce)cf.1943-5509.0000305

[6] Liu, C., Yan, C., Zheng, G., Zhao, B., & Liu, Y., "Field testing of seismic performance of prestressed high strength concrete piles reinforced with non-prestressed tendons considering pile–soil interaction", Soil Dynamics and Earthquake Engineering, 2023, 174 : p. 108190. DOI: https://doi.org/10.1016/j.soildyn.2023.108190

[7] Yao, Y., Hong, B., Liu, X., Wang, G., Shao, Z., & Sun, D., "Field and Numerical Study of the Bearing Capacity of Pre-Stressed High-Strength Concrete (PHC)-Pipe-Pile-Reinforced Soft Soil Foundations with Tie Beams", Applied Sciences, 2023, 13(21): p. 11786. DOI: https://doi.org/10.3390/app132111786

[8] Xu, Y., Chen, Z., Fan, J., Li, Z., Zhang, K., & Tu, X., "Study on the flexural performance of prestressed concrete solid square piles and resilient clamping connections", KSCE Journal of Civil Engineering, 2023, 27(1): p. 285-298. DOI: https://doi.org/10.1007/s12205-022-0148-8

[9] Liang, J., Tang, X., Lin, W., Yu, Y., Li, J., & Fan, Z., “Innovative design of pipe piles combined both the effect of pile foundation and composite foundation for soft soil treatment”, Japanese Geotechnical Society Special Publication, 2020, 8(13): p. 547-552. DOI: https://doi.org/10.3208/jgssp.v08.c62

[10] Wang, R., Li, Y., Liu, X., Zhang, S., Zhang, C., Li, Z., & Wang, P., "Research on advantages and disadvantages of prestressed concrete hollow square pile and pipe pile in pile foundation selection", IOP Conference Series: Earth and Environmental Science, 2021, 787(1): p. 012022.DOI: https://doi.org/10.1088/1755-1315/787/1/012022

[11] Xu, W., Miao, H., & Chen, Y., "Pull-out behavior and damage assessment of core concrete of Full-scale prestressed High-strength hollow square piles", Structures, 2023, 51: p. 1906-1918. DOI: https://doi.org/10.1016/j.istruc.2023.03.159

[12] Statkus, T., Norkus, A., & Mikolainis, M., “Experimental investigation of settlement in sand soil of jacked pile subjected by vertical compressive cyclic loading”, Procedia Engineering, 2017, 172: p1053-1058. DOI: https://doi.org/10.1016/j.proeng.2017.02.162

[13] Liu, H.T., Sun, J., “Study on Pressing Pipe Pile into Complicated Foundation”, IOP Conference Series: Earth and Environmental Science, 2021, 621(1): p. 012057. DOI: https://doi.org/10.1088/1755-1315/621/1/012057

[14] Lu, W.Y., “Study on the bearing performance of precast pile for lead hole implantation under complex formation conditions (in Chinese)”, Heilongjiang University, 2023. DOI: https://doi.org/10.27123/d.cnki.ghlju.2023.000501

[15] Li, S., Wang, K., Shao, M.X., Zeng, X., “Technical scheme and application of pile foundation reinforcement for a high-rise building under construction”, Building Structure, 2021, 51(08): p. 115-118+131. DOI: https://doi.org/10.19701/j.jzjg.2021.08.019

[16] Kou, H. L., Chu, J., Guo, W., & Zhang, M. Y., "Field study of residual forces developed in pre-stressed high-strength concrete (PHC) pipe piles", Canadian Geotechnical Journal, 2016, 53(4): p. 696-707. DOI: https://doi.org/10.1139/cgj-2015-0177

[17] Xiao, Z.R., Wang, Y.L., Zhao, X.Q., Jiang, M.M., Zhao, W.C., “Experimental investigation on resistance and response of jacked model piles in sand”, Journal of Building Structures, 2022, 43(11): P. 294-302. DOI: https://doi.org/10.14006/j.jzjgxb.2020.0793

[18] Zhu, Y.Y., Xiao, Z.R., “Analysis of Pile End Resistance of Static-Pressure Pile in Sandy Foundation”, Journal of Tangshan University, 2023, 36(03): p. 9-14. DOI: https://doi.org/10.16160/j.cnki.tsxyxb.2023.03.002

[19] Budek, A. M., & Priestley, M. J. N., "Experimental analysis of flexural hinging in hollow marine prestressed pile shafts", Coastal Engineering Journal, 2005, 47(1): p. 1-20. DOI: https://doi.org/10.1142/S0578563405001161

[20] Kai, Y., "The research on static performance of prestressed high-strength concrete pipe pile (PHC pile) and application engineering", Hefei University of Technology, 2017. DOI: https://doi.org/10.27101/d.cnki.ghfgu.2017.000009

[21] Filho, J. M., Moura, A. S., & Monteiro, F. F., "Performance control of root piles using a digital odometer", DYNA, 2022, 89(220): p.64-71. DOI: https://doi.org/10.15446/dyna.v89n220.95008

[22] de Jesus Souza, T., Querelli, A., de Souza Cruz, F. V. A., & Trejo-Noreña, P. C., "Use of the dynamic load test to obtain the pile capacity –the Brazilian experience", DYNA, 2021, 88(217): p. 169-177. DOI: https://doi.org/10.15446/dyna.v88n217.93416

[23] Khanmohammadi, M., Armaghani, D. J., & Sabri Sabri, M. M., "Prediction and Optimization of Pile Bearing Capacity Considering Effects of Time", Mathematics, 2022, 10(19): p. 3563. DOI: https://doi.org/10.3390/math10193563

[24] JGJ 94. Technical Code for Building Pile Foundations. National Standard of the People's Republic of China. 2008. Available online: http://www.doc88.com/p-8969117080669.html (accessed on 1 June 2020).

[25] Kézdi, Á., & Rétháti, L. Soil mechanics of earthworks, foundations, and highway engineering, Elsevier, 3, 1988. DOI: https://doi.org/10.1016/B978-0-444-98929-1.50006-0

[26] Wei, Y., Wang, D., Li, J., Jie, Y., Ke, Z., Li, J., & Wong, T., "Evaluation of ultimate bearing capacity of pre-stressed high-strength concrete pipe pile embedded in saturated sandy soil based on in-situ test", Applied Sciences, 2020, 10(18): p. 6269. DOI: https://doi.org/10.3390/app10186269

[27] Patrick Schober., Christa Boer., Lothar A. Schwarte., "Correlation Coefficients: Appropriate Use and Interpretation", Anesthesia & Analgesia, 126(5): p 1763-1768, May 2018. DOI: https://doi.org/10.1213/ane.0000000000002864

[28] Wu, P.F., "Experimental Study on Strength Characteristics of the Frozen Soil-pile Interface and Numerical Simulation Analysis on Bearing Capacity of Pile Foundation in Permafrost Region", China Mining University, 2021. DOI: https://doi.org/10.27623/d.cnki.gzkyu.2021.002103

[29] Ponomarev, A. B., Akbulyakova, E. N., & Ofrichter, Y. V., "Prediction of bearing capacity of driven piles in semi-rocky soils", Soil Mechanics and Foundation Engineering, 2020, 57(2): p. 133-138. DOI: https://doi.org/10.1007/s11204-020-09648-1

[30] Yang, Z., & Wang, W., "Experimental and numerical investigation on the behaviour of prestressed high strength concrete pile-to-pile cap connections", KSCE Journal of Civil Engineering, 2016, 20: p. 1903-1912. DOI: https://doi.org/10.1007/s12205-015-0658-8

[31] Wang, S. M., & Yin, X. S., "Study on Seismic Performance of C105 Prestressed High Strength Concrete Hollow Pipe Pile", Materials Science Forum, 2020, 980: p. 282-290. DOI: https://doi.org/10.4028/www.scientific.net/MSF.980.282

[32] Siemaszko, P., & Meyer, Z., "Analysis of the pile skin resistance formation", Studia Geotechnica et Mechanica, 2021, 43(4): p.380-388. DOI: https://doi.org/10.2478/sgem-2021-0026

[33] Vural, İ., Kabaca, H., & Poyraz, S., "A Novel Approach Proposal for Estimation of Ultimate Pile Bearing Capacity Based on Pile Loading Test Data", Applied Sciences, 2023, 13(13): p. 7993. DOI: https://doi.org/10.3390/app13137993